Mon. Not. R. Astron. Soc. **000**, 000–000 (0000) Printed 1 February 2008 (MN LaTeX style file v1.4)

arXiv:astro-ph/0006311v1 21 Jun 2000

Properties of observed Ly-α forest

M. Demiański[1,2], A.G. Doroshkevich[3,4], & V.Turchaninov[4]
1*Institute of Theoretical Physics, University of Warsaw, 00-681 Warsaw, Poland*
2*Department of Astronomy, Williams College, Williamstown, MA 01267, USA*
3*Theoretical Astrophysics Center, Juliane Maries Vej 30, DK-2100 Copenhagen Ø, Denmark*
4*Keldysh Institute of Applied Mathematics, Russian Academy of Sciences, 125047 Moscow, Russia*

Accepted ..., Received ..., in original form ... .

ABSTRACT

The main observed properties of Ly-α absorbers are investigated on the basis of theoretical model of formation and evolution of DM structure elements. This model is generally consistent with simulations of absorbers formation and with statistical description of structure evolution based on the Zel'dovich theory. The analysis of redshift variations of comoving linear number density of absorbers was performed in our previous paper.

We show that the observed characteristics of Doppler parameter can be related to the size of DM structure elements what allows us to explain the observed distribution of Doppler parameter. This distribution is found to be consistent with the Gaussian initial perturbations. The observed characteristics of entropy and column density, N_{HI}, confirm that merging of pancakes is the main evolutionary process at redshifts $z \geq 2$. The observed sample of absorbers characterizes mainly the matter distribution within large low density regions and therefore it is difficult to reconstruct the density field from the distribution of absorbers.

Key words: cosmology: large-scale structure of the Universe — quasars: absorption: general — surveys.

1 INTRODUCTION

The intergalactic nature of Ly-α forest was established by Sargent et al. (1980) and later many models of absorbers formation and evolution were proposed (see, e.g., Rees 1986, 1995; Ikeuchi & Ostriker 1986; Bond, Szalay & Silk 1988; Miralda-Escude et al. 1996; Hui et al. 1997; Nath 1997; Valageas, Schaeffer, & Silk 1999). The essential progress was reached through simulations of dynamical and thermal evolution of gaseous component with the CDM-like power spectrum which is probably responsible for the formation of observed galaxy distribution. Such simulations (Petitjean et al. 1995; Hernquist et al. 1996; Bond & Wadsley 1997; Zhang et al. 1997, 1998; Theuns et al. 1998, 1999; Bryan et al. 1999; Davé et al. 1999; Weinberg et al. 1998; Machacek et al. 2000) reproduce successfully the main observed properties of absorbers and connect this problem with a more general problem, that is the nonlinear evolution of initial perturbations and formation of large scale matter and observed galaxy distribution. This progress allows us to consider the properties of absorbers in the context of nonlinear theory of gravitational instability and statistical description of formation and evolution of DM structure (Zel'dovich 1970; Shandarin & Zel'dovich 1988; Demiański & Doroshkevich 1999, hereafter DD99; Demiański et al. 2000, hereafter DDMT).

It is commonly recognized that in the DM dominated universe the fundamental properties of observed matter distribution are determined by the evolution of DM structure elements. The approximate statistical description of expected characteristics of DM structure elements based on the Zel'dovich theory was given in DD99 and DDMT for the CDM-like transfer function (Bardeen et al. 1986) and the Harrison – Zel'dovich initial power spectrum. This process can be outlined as a random formation and merging of Zel'dovich pancakes, their successful transformation to filamentary component of structure, and the hierarchical merging of both pancakes and filaments to form rich walls. All steps of this evolution are driven by the initial power spectrum.

Some results of this statistical description were compared with simulations at small redshifts (DD99, Doroshkevich et al., 1999, hereafter DMRT; DDMT). This comparison shows that the main simulated and observed structure characteristics are consistent with the theoretical expectations. Here we use this approach for the analysis and interpretation of the absorbers observed at large redshifts as a Ly$-\alpha$ forest, and we show that some of the observed characteris-

© 0000 RAS

tics of Ly-α absorbers can also be successfully described in the framework of this theoretical model.

The validity of this description, when it is applied to structure at high redshifts, is not yet reliably verified with available simulations due to a small density contrast of poor structure elements dominating at higher redshifts. The first tests revealed, however, the existence of three kinds of structure elements, namely, high density filaments, clumps, and low density pancakes in DM spatial distribution at $z = 3$. The theoretical description (DD99) confirms also the self-similar character of structure evolution (at least when the Zel'dovich approximation can be applied). More detailed statistical comparison of absorbers characteristics simulated at high redshifts with theoretical expectations is however required.

Such approach implies more traditional investigation of properties of discrete absorbers rather then a continuous non-linear line-of-sight density field (see, e.g., Weinberg et al. 1998) and, so, we will concentrate more attention on statistics of discrete absorbers. The observations of galaxies at large redshifts verifies that strong nonlinear compression of DM and gaseous components occurs even at $z \approx 3-5$ and earlier (Steidel et al. 1998; Dey & Chaffee 1998; Fan et al. 2000) and, so, discrete high density absorbers can already exist at such redshifts. This approach allows us to reach more clarity in the description of formation and evolution of structure and to establish correlations between properties of observed absorbers and invisible DM component.

It can be expected that absorbers are predominantly related to the more numerous population of moderately rich pancakes and to periphery of richer pancakes and filaments. This means that information obtained from such traditional methods of analysis is related with the extended lower density regions of the universe rather then with the rich wall-like condensations. In this respect, the absorbers characteristics are complementary to the information obtained from the analysis of large scale galaxy distribution. In order to discriminate between properties of absorbers that can be associated with the evolution of DM component and are specific of the gaseous component it is necessary to compare the expected characteristics of DM structure and observed discrete Ly-α absorbers. Thus, some fraction of weaker absorbers formed within expanded regions is not connected with the DM structure (Bi & Davidsen 1997; Zhang et al. 1998; Davé et al. 1999). Such comparison reveals also the potential and limitations of this approach.

This approach relies on identification of separate absorbers in the observed spectra what restricts the number of available spectra. Moreover, properties of some of the identified lines can be distorted due to superposition of several lines and cannot be reliably discriminated from the influence of diffuse intergalactic gas (McGill 1990; Levshakov & Kegel 1996, 1997) what introduces some additional uncertainties in our analysis. Our study of simulations at small redshifts (DDMT) shows, however, that the influence of the last effect depends on the power spectrum of primordial perturbations and for the CDM-like power spectrum, at moderate redshifts, its impact is not very strong. This problem should be investigated in more details using the available simulations of absorbers.

The redshift dependence of linear number density of absorbers was discussed in Demiański, Doroshkevich & Turchaninov (2000, hereafter Paper I) under the assumption that the neutral hydrogen traces the potential wells formed by DM pancakes. This model is similar, in some respects, to previously discussed theoretical and simulated models referred above. In this paper we show that this model provides a reasonable self consistent description and interpretation of other observed properties of absorbers and demonstrates that merging of earlier formed structure elements plays an important role in the evolution of absorbers. This approach makes it possible to approximately discriminate between the evolution of DM structure elements and faster and randomly perturbed evolution of gaseous component, that is suitably described by the evolution of entropy of compressed gas, and to specify the main factors responsible for it. In particular, we can roughly discriminate between adiabatic and shock formation of absorbers and show that the adiabatic processes may be not very important, at least for the formation of stronger *observed* absorbers. Properties of observed absorbers demonstrate the important role of merging of earlier formed structure elements for the absorber evolution. Our method gives reasonable fits for the observed distribution of Doppler parameter, b, and hydrogen column density, N_{HI}, and connects them with the basic cosmological parameters, Ω_m & h, and the amplitude of initial perturbations. Our main results are consistent with conclusions of Zhang et al. (1998), Weinberg et al. (1998) and Davé et al. (1999). Some differences between the theoretical expectations and simulations will be discussed below.

The theory cannot yet describe in details the relaxation of compressed matter, the disruption of structure elements caused by the gravitational instability of compressed DM and the distribution of neutral hydrogen across DM pancakes. Therefore, in this paper several parameters characterizing the properties of DM and neutral hydrogen distribution remain undetermined. They can be estimated by applying the discussed methods to simulations that provide an unified physical picture of absorber formation and evolution.

The composition of observed absorbers is complicated and if at low redshifts a significant number of stronger Ly-α lines and metal systems is associated with galaxies (Bergeron et al. 1992; Lanzetta et al. 1995; Cowie et al. 1995; Tytler et al. 1995; Le Brune et al. 1996) then the population of weaker absorbers dominates at higher redshifts and mainly disappears at redshift $z \leq 2$. It is not observed by other methods and can be associated with the population of weaker structure elements formed by non luminous baryonic and DM components and situated in extended lower density regions. Some number of weak Ly-α lines observed even at small redshifts far from galaxies (Morris et al. 1993; Stocke et al. 1995; Shull et al. 1996) can be considered as a trace of this population.

An interesting problem arises, namely the possible reconstruction of spatial DM distribution using the redshift distribution of absorbers. Two methods of such reconstruction were proposed by Weinberg et al. (1998) and Nusser & Haehnelt (1998). Here we examine the method based on one dimensional smoothing of density field. We show that results depend strongly on the used sample of absorbers and on the method of identification of properties of DM component of absorbers. Interpretation of results of such reconstruction is now questioned and more detailed investigation of this problem is required.

Simulations of structure evolution take into account the impact of many important factors together and provide an unified picture of absorber formation and evolution. But so far such simulations can be performed only in small boxes what introduces artificial cutoffs in the power spectrum and makes the investigation of large scale structure evolution difficult. Such simulations cannot yet reproduce all important features of interactions of small and large scale perturbations and the direct analysis of the observed absorbers characteristics might now be more perspective in this respect. Indeed, the large scale modulation of redshift distribution of Ly-α lines found by Cristiani et al. (1996) and strong nonhomogeneities found at $z \leq 2$ by Williger et al. (1996), Quashnock et al. (1996, 1998), and Connolly et al. (1996) could be attributed to the extremely rich structure elements which are not yet found in simulations.

This paper is organized as follows. The theoretical model of the structure evolution is discussed in Secs. 2. Sec. 3 contains information about the used observational databases. The results of statistical analysis are given in Sec. 4, 5 & 6. Discussion and conclusion can be found in Sec. 7.

2 MODEL OF STRUCTURE EVOLUTION.

The main observational characteristics of absorption lines are the redshift, z_{abs}, the column density of neutral hydrogen, N_{HI}, and the Doppler parameter, b. On the other hand, the theoretical description of structure formation and evolution is dealing with the linear number density, $n_{abs}(z)$, temperature, T, density of DM and entropy of gaseous components, and with the ionization degree of hydrogen. To connect these theoretical and observed parameters a physical model of absorbers formation and evolution is required.

Broad set of such models was discussed during last twenty years (see references above). Here we repeat some of the assumptions already discussed in earlier publications. Our consideration is based on the statistical description of formation and evolution of DM structure in CDM-like models (DD99, DDMT), and it is compared with observed and simulated spatial distributions of DM component and galaxies at small redshifts.

2.1 Physical model of absorbers.

Here we consider a simple self-consistent model of the absorbers formation and evolution based on the Zel'dovich approximation. We assume that:

(i) The DM distribution forms an interconnected structure of sheets (Zel'dovich pancakes) and filaments, their main parameters are approximately described by the Zel'dovich approximate theory applied to CDM-like initial power spectrum (DD99, DDMT). The richer DM pancakes can be relaxed, long-lived, and approximately stationary.

(ii) Gas is trapped in the gravitational potential wells formed by the DM distribution. The gas temperature and observed Doppler parameter, b, trace the depth of the DM potential wells.

(iii) For a given temperature the gas density within the wells is determined by the gas entropy created during the previous evolution. The gas entropy changes, mainly, due to the shocks heating in the course of merging of pancakes and, possibly, due to the bulk heating produced by local sources.

(iv) The ionization of the gas is caused by the outer radiation field and for the majority of absorbers ionization equilibrium is assumed.

(v) The evolution of observed properties of absorbers is mainly caused by merging, transversal compression and/or expansion and disruption of DM pancakes. Possible bulk heating of the trapped gas and possible variations of the intensity and spectrum of the ionizing UV radiation field can be also important and will provide the fine-tuning between the observed and expected properties of absorbers.

(vi) In the context of the simple model we identify the velocity dispersion of DM component compressed within pancakes with the temperature of hydrogen and the Doppler parameter b of absorbers. We consider the possible macroscopic motion within pancakes as subsonic and assume that they cannot essentially distort the measured Doppler parameter.

The formation of sheet-like DM structure elements (Zel'dovich pancakes) as an inevitable first step of evolution of small DM perturbations was certainly established both by theoretical considerations (Zel'dovich 1970; Shandarin & Zel'dovich 1989; in DD99 for CDM-like power spectrum) and numerically (Shandarin et al. 1995). Here we will restrict our consideration to the subpopulation of slowly evolving DM pancakes when their column density remains almost the same during the time comparable with $H^{-1}(z)$. In the opposite case, when rapid expansion of matter in the transversal directions takes place, the pancake is eroded and N_{HI} decreases below the observational limit. The rapid compression transforms pancakes into filaments that is another subpopulation of observed Ly-α absorbers. These short-lived pancakes can be mainly identified with a subpopulation of weaker absorbers with a column density $N_{HI} \leq 10^{13} cm^{-2}$ dominated at higher redshifts $z \geq 3$.

The subpopulation of weaker absorbers also contains "artificial" caustics (McGill 1990) and absorbers identified with slowly expanding underdense regions (Bi & Davidsen 1997; Zhang et al. 1998; Davé et al. 1999). These kinds of absorbers are not connected with DM structure and produce noise, which is stronger at higher redshifts $z \geq 3$.

Further on, even our approximate consideration cannot be applied to filaments and high density clumps, when both the gravitational potential and the gas temperature along a line of sight depend essentially on the matter distribution across this line. So, our investigation has to be restricted to the subpopulation of DM composed sheet-like structure elements. This means that the appropriate subsample of observed absorbers has to be considered.

Fortunately, the correlations between observed parameters b and N_{HI} and evolutionary rate of observed linear number density of absorbers discussed in Paper I allows us to discriminate statistically the filamentary and sheet-like dominated subpopulations of absorbers and to perform approximately such selection. Thus, it may be expected that the sheet-like DM composed absorbers dominate for $b \geq 17$ – 20km/s and $10^{13} cm^{-2} \leq N_{HI} \leq 10^{14} cm^{-2}$.

Both theoretical analysis and simulations show the successive transformation of sheet-like elements into filamentary-like ones and, at the same time, the merging of both sheet-like and filamentary elements into richer sheets or walls. Such continual transformation of structure goes on all the time. These processes imply the existence of complicated time-dependent internal structure of high density elements and, in particular, the essential arbitrariness in discrimination of such elements into filaments and sheets. The morphology of structure elements can be quantitatively characterized with new powerful techniques such as the Minimal Spanning Tree analysis (DMRT, DDMT) and the Minkowski Functional (Sathyaprakash et al. 1998; Kerscher 1999). Such an analysis applied to observed and simulated catalogues demonstrates the continual distribution of morphological characteristics with a relatively small fraction of distinct high density filaments and elliptical clumps, and allows to estimate the degree of filamentarity and sheetness of both individual elements and sample as a whole.

In this paper, as was noted above, we use the term 'pancake' for structure elements with relatively small gradient of properties (first of all temperature) across a line of sight. With such a criterion, the anisotropic halo of filaments and clumps can also be considered as 'pancake-like'. At the same time, as was discussed in Paper I, the evolutionary rate of observed linear number density of such absorbers can be similar to that typical for filaments or clumps. By imposing some restrictions on the observed b and N_{HI} it is possible to improve the statistical discrimination of these components, but even then the selection is not unique. More detailed investigation of observed and simulated properties of absorbers is required to improve the selection criteria and to prepare more adequate physical model of absorbers.

2.2 DM structure elements and Doppler parameter.

Among the observed characteristics of Ly-α absorbers the Doppler parameter, b, is more closely linked with properties of DM component. In this section we introduce some relations between characteristics of DM pancakes and the b parameter based both on the theoretical arguments and analysis of simulated DM and observed galaxy distribution at small redshifts. Some properties of such high density DM walls formed at the redshift $z \ll 1$ were analyzed in DMRT, DD99 and DDMT. In this Section relations between basic characteristics of DM pancakes are introduced (without proofs) as a basis for further analysis.

The fundamental characteristics of DM pancakes are the dimensionless Lagrangian thickness, q, and the DM column density, μ_f:

$$\mu_f \approx \frac{\rho_f l_0 q}{(1+z_f)} = \frac{3H_0^2}{8\pi G} l_0 \Omega_m (1+z_f)^2 q, \qquad (2.1)$$

$$l_0 \approx \frac{6.6}{h\Omega_m} h^{-1}\mathrm{Mpc} = \frac{59.4\mathrm{Mpc}}{\Theta_m}, \quad \Theta_m = 9\Omega_m h^2,$$

where Ω_m is the dimensionless mean matter density of the universe and H_0=100 h km/s/Mpc is the Hubble constant. The Lagrangian thickness of a pancake, $l_0 q$, is defined as an unperturbed distance at redshift $z = 0$ between positions of DM particles bounding the pancake.

2.2.1 *DM pancakes in Zel'dovich approximation.*

The expected probability distribution function (PDF) for the Lagrangian thickness of a pancake, q, can be written (DD99) as

$$N_q \approx \frac{1}{4\tau^2\sqrt{\pi}} \cdot e^{-\xi}\, \frac{\mathrm{erf}(\sqrt{\xi})}{\sqrt{\xi}}, \quad \xi = \frac{q}{8\tau^2}, \qquad (2.2)$$

$$< \xi > = 0.5 + 1/\pi \approx 0.82, \quad \langle \xi^2 \rangle = 0.75 + 2/\pi \approx 1.39$$

where the dimensionless 'time' $\tau(z)$ describes the evolution of perturbations in the Zel'dovich theory (Appendix A). More details are given in DMRT, DD99 and DDMT.

In the Zel'dovich theory the Lagrangian thickness of DM pancake, q, is closely linked to the velocity of infalling matter, v_{inf}, the thickness, h_{DM}, and overdensity, δ_{DM}, of compressed dark matter (DDMT):

$$\langle v_{inf} \rangle \approx \frac{H(z) l_0 \beta(z)}{2(1+z)} q, \quad \sigma_{inf} \approx \frac{l_0 H(z)}{(1+z)} \tau [1+\beta(z)] \sqrt{\frac{q}{3}},$$

$$\beta(z) = \frac{1+z}{\tau} \left| \frac{d\tau}{dz} \right|, \qquad (2.3)$$

$$\langle h_{DM} \rangle \ll \sqrt{\langle h_{DM}^2 \rangle} \approx \frac{2 l_0 \tau}{1+z} \sqrt{q}, \quad \delta_{DM} \approx \frac{\sqrt{q}}{2\tau}.$$

The PDF of infalling velocity is Gaussian for Gaussian initial perturbations (DD99, DDMT) with the mean value and dispersion as given by (2.3).

Further on we will identify the kinetic energy accumulated by the DM pancake with the Doppler parameter, b_{DM}, and with the *observed* Doppler parameter, b. We will assume that

$$b_{DM}^2 = \langle v_{inf}^2 \rangle \approx \frac{l_0^2 H^2(z) q}{12(1+z)^2} (q\beta^2(z) + 4\tau^2 [1+\beta(z)]^2). \qquad (2.4)$$

This assumption is valid during some time after formation of the pancake and allows us to reasonably describe the observed properties of absorbers. Later on, other processes such as the relaxation and small scale clustering of compressed matter, as well as, the pancake compression and/or expansion in transversal directions become important. Some of them will be discussed below.

For larger redshifts, $z \geq 2$, $q \ll 1$, we can introduce more suitable notation separating out large numerical factors. We can take with a reasonable precision

$$H(z) \approx H_0 (1+z)^{3/2} \sqrt{\Omega_m} \approx 267 \zeta^{3/2} \sqrt{\Theta_m} km/s/\mathrm{Mpc},$$

$$\tau \approx 0.06 \zeta^{-1} \tau_z, \quad \beta \approx 1, \quad \zeta = 0.25(1+z), \qquad (2.5)$$

what allows us to rewrite (2.3) and (2.4) more transparently as

$$b_{DM} \approx b_0 \sqrt{\xi^2 + 2\xi}, \quad \xi = \eta^2 (1 + \sqrt{1+\eta^2})^{-1}, \quad \eta = b_{DM}/b_0,$$

$$\langle b_{DM} \rangle \approx 1.43 b_0, \quad \langle b_{DM}^2 \rangle \approx 3 b_0^2, \quad \delta_{DM} \approx \sqrt{2\xi}, \qquad (2.6)$$

$$b_0 = 33 km/s \zeta^{-3/2} \tau_z^2 \Theta_m^{-1/2} \Theta_v,$$

where ξ was introduced by (2.2), and the factor $\Theta_v \sim 1$ describes differences between (2.4) and (2.6).

These relations connect the velocity dispersion within DM pancakes with their DM column densities and allow to obtain (using the PDF (2.2)) the expected PDF for b_{DM} as follows:

$$N_b = N_q \cdot \frac{dq}{db_{DM}} = \frac{2}{b_0\sqrt{\pi}}\; e^{-\xi}\frac{\sqrt{2+\xi}}{1+\xi}\; \mathrm{erf}(\sqrt{\xi}). \qquad (2.7)$$

2.2.2 Relaxation of DM pancakes.

The analysis of simulations (DDMT) shows that in rich pancakes the DM particles are relaxed and gravitationally confined, and such pancakes are long-lived and (quasi)stationary. The relaxation of DM particles is essentially accelerated by the small scale clustering of compressed matter and leads to evaporation of particles with larger velocities, what restricts the observed Doppler parameter of rich pancakes. Thus, for observed and simulated galaxy walls, at small redshifts, $b \sim 300 - 350$km/s is found to be more typical.

The approximate relation for the velocity dispersion of DM particles within relaxed pancakes can be written as follows:

$$b_{DM} \approx \epsilon(z)\sqrt{\langle b^2_{DM}\rangle}\left(\frac{q}{\langle q\rangle}\right)^{\gamma} \approx \epsilon(z)\sqrt{3}\left(\frac{q}{\langle q\rangle}\right)^{\gamma}, \qquad (2.8)$$

$$\langle\epsilon\rangle \approx 0.3 - 0.7, \quad \gamma \approx 0.6 - 0.7.$$

Here the random dimensionless parameter $\epsilon(z)$ describes the lost of energy in the course of relaxation. Estimates of the factors γ and ϵ can be refined through a more detailed comparison with simulations.

For relaxed pancakes, instead of (2.6) & (2.7) we obtain that, for example, for $\gamma = 2/3$, the expected characteristics of Doppler parameter can be taken as follows:

$$\langle q^{2/3}\rangle \approx 1.2\langle q\rangle^{2/3}, \quad \langle b_{DM}\rangle \approx 2b_0\epsilon, \quad q \approx 8\tau^2\left(\frac{\eta}{2\epsilon}\right)^{3/2},$$

$$N_b \approx \frac{3}{\sqrt{\pi}b_0\epsilon}\exp(-\xi)\frac{\mathrm{erf}(\sqrt{\xi})}{\xi^{1/6}}, \quad \xi = \left(\frac{\eta}{2\epsilon}\right)^{3/2}. \qquad (2.9)$$

Relations (2.2), (2.7) and (2.9) link the observed Doppler parameter with the pancake DM column density, q, and indicate that the distribution function of Doppler parameter is similar to a gamma distribution. These relations take into account the successive merging of earlier formed structure elements – both filaments and pancakes – what leads, in particular, to formation of observed galaxy walls at small redshifts.

As was discussed in Paper I, rapid expansion of pancakes in transversal directions decreases N_{HI} below the observational limit of $N_{HI} \sim 10^{12} cm^{-2}$. Some fraction of such expanded pancakes with smaller N_{HI} can be observed. The rapid compression of a pancake along one or both of the transversal directions decreases its surface area and also the probability to see such a pancake as an absorber.

These inferences are based on theoretical arguments tested on simulated formation of walls at small redshifts. More accurate estimates of possible distortions can be obtained through comparison with representative simulations at high redshifts.

As was noted above, we identify b_{DM} as given by (2.6) or (2.8) with the *observed* Doppler parameter, b.

2.3 Large scale absorber distribution

The observed spatial distribution of absorbers is very similar to the Poissonian distribution. Even so, the large scale modulation of absorbers distribution is an interesting characteristic. If absorbers are actually linked to the DM distribution as was discussed in Sec. 2.2, then it can be expected that this modulation will be later transformed – due to the gravitational instability – to the galaxy distribution observed at small redshifts as large and superlarge scale structure.

The large scale matter distribution can be conveniently characterized by the one dimensional smoothed density field. The required variance of density can be expressed through the dimensionless moments of initial power spectrum, $p(k)$. Thus, for the density smoothed over a scale r_s with a Gaussian window function we have:

$$\sigma^2_\rho(r_s) = (2\pi)^{-3}\int d^3k\; \exp[-(\mathbf{k}\mathbf{r}_s)^2]\; p(k)$$

$$= \frac{1}{4\pi^{3/2}r_s}\int_0^\infty dk\; kp(k)\; erf(kr_s), \qquad (2.10)$$

where k is a comoving wave number. For $r_s \to \infty$

$$\sigma^2_\rho(r_s) \approx \frac{1}{4\pi^{3/2}r_s}\int_0^\infty dk\; kp(k) = \frac{\kappa^2_{cdm}}{4\pi^{3/2}r_s}\int_0^\infty dk\; kp_{cdm}(k),$$

where p_{cdm} is the standard CDM-like power spectrum with the Harrison-Zel'dovich asymptotic $p(k) \propto k, as\;\; k \to 0$ and the CDM transfer function and κ_{cdm} describes the impact of possible deviations of actual and CDM-like power spectra used for numerical estimates. For large r_s we have:

$$\sigma^2_\rho(r_s, z) \approx 18\kappa^2_{cdm}\tau^2(z)\frac{l_0}{r_s},$$

$$\tau = \tau_\rho \approx 0.24\sqrt{\frac{r_s}{l_0}}\frac{\sigma_\rho(r_s,z)}{\kappa_{cdm}}\left(1 + \frac{0.1l_0}{r_s}\right)^{1/6}. \qquad (2.11)$$

For such estimates we will use the measured redshift of absorbers and relations (2.6) and (2.9) to obtain the required DM column density of absorbers through the measured Doppler parameter, b.

Such approach is similar but not identical to that used by Weinberg et al. (1998) and Nusser & Haehnelt (1998).

2.4 Properties of gaseous structure elements.

If the observed Doppler parameter characterizes the basic properties of DM pancakes then the hydrogen column density characterizes the state of the gaseous component trapped by the DM pancakes. The gas density and the hydrogen column density are sensitive to many factors. Firstly, the radiation field provides the high ionization and bulk heating of hydrogen. Secondly, the shock compression and heating of gas accompany the process of merging of richer DM pancakes. The adiabatic compression or expansion of gas changes also its temperature and the observed hydrogen column density.

The suitable characteristic of the state of gas is its entropy. It remains constant during the adiabatic compression and expansion of gas and it increases due to all irreversible processes such as the shock and bulk heating. The entropy decreases only due to the radiative cooling which is usually moderate. When gas temperature is rigidly bounded by the gravitational potential of DM distribution the entropy and the gas density are closely linked.

2.4.1 Properties of homogeneously distributed hydrogen

The properties of compressed gas can be suitably related to better known parameters of homogeneously distributed gas, which were described in many papers (see, e.g., Ikeuchi & Ostriker 1986). In this case the baryonic density and the temperature can be taken as

$$\bar{n}_b = 1.2\cdot 10^{-5}\Omega_b h^2 (1+z)^3 cm^{-3} = n_0\zeta^3,$$

$$n_0 = 1.5\cdot 10^{-5} cm^{-3}\Theta_{bar},\quad \Theta_{bar} = \Omega_b h^2/0.02, \qquad (2.12)$$

$$T_{bg}\approx 1.6\cdot 10^4 K,\quad b_{bg}\approx 16\text{km/s},\qquad \zeta = \frac{(1+z)}{4},$$

and the entropy of the gas can be characterized by the function

$$F_{bg} = T_{bg}/\bar{n}_b^{2/3} = F_0\zeta^{-2},\quad F_0\approx 2\ \text{kev}\cdot\text{cm}^2\Theta_{bar}^{-2/3}. \quad (2.13)$$

For reference, the typical entropy of the primordial gas before reheating, F_{prm}, and of gas observed in galaxies, F_{gal}, and in clusters of galaxies, F_{cl}, are:

$$F_{prm}\sim 3\cdot 10^{-5}\ \text{kev}\cdot\text{cm}^2\approx 1.5\cdot 10^{-5}F_0$$

$$F_{gal}\sim 10^{-3}\text{kev}\cdot\text{cm}^2\approx 10^{-3}F_0$$

$$F_{cl}\sim 300\text{kev}\cdot\text{cm}^2\approx 150 F_0$$

These data illustrate the range of observed variations of gaseous entropy.

2.4.2 The hydrogen column density and entropy of absorbers.

The observed column density of neutral hydrogen can be written as an integral over pancake along a line of sight

$$N_{HI} = \int dx\frac{dN_{bar}}{dx}x_H = \langle N_{bar}\rangle\langle x_H\rangle\kappa. \qquad (2.14)$$

Here $\langle N_{bar}\rangle$ is the mean column density of baryons across the absorber, $\langle x_H\rangle$ is the mean fraction of neutral hydrogen and the dimensionless parameter κ characterizes the nonhomogeneous distribution of neutral hydrogen across absorber. We will assume that both DM and gaseous components are compressed together and, so, the column density of baryons and DM component are approximately proportional to each other. Therefore, we can take

$$\langle N_{bar}\rangle\approx\frac{\bar{n}_b l_0 q}{\nu(1+z)}\approx 2.1\cdot 10^{19}cm^{-2}\ \xi(b)\frac{\tau_z^2\Theta_{bar}}{\nu\Theta_m},$$

$$\langle\Delta r\rangle\langle\delta_{bar}\rangle = 0.25 l_0 q\zeta^{-1}\approx 0.5\xi(b)\tau_z^2\zeta^{-3}\text{Mpc}. \qquad (2.15)$$

Here $\langle\Delta r\rangle$ and $\langle\delta_{bar}\rangle$ are the mean proper thickness and overdensity of compressed gas above the mean density, $\xi(b)$, τ_z&ζ are given by (2.2) & (2.5), $\nu = \cos\varphi$ describes the random orientation of absorbers and the line of sight, and expressions (2.7) & (2.9) link functions q, b and τ.

Under the assumption of ionization equilibrium of the gas within a DM pancake and neglecting a possible contribution of macroscopic motions to the b-parameter ($T\propto b^2$), the fraction of neutral hydrogen is

$$\langle x_H\rangle = n_0\zeta^3\langle\delta_{bar}\rangle\frac{\alpha_{rec}(T)}{\Gamma_\gamma} = x_0\frac{\langle\delta_{bar}\rangle}{\Gamma_{12}}\zeta^3\left(\frac{b_{bg}}{b}\right)^{3/2},$$

$$\Gamma_\gamma = \Gamma_{12}\cdot 10^{-12}s^{-1},\quad x_0 = 4.1\cdot 10^{-6}\Theta_{bar}.$$

The recombination coefficient, $\alpha_{rec}(T)$, and the photoionization rate due to the extragalactic UV background radiation, Γ_γ, are taken as

$$\alpha_{rec}(T)\approx 4\cdot 10^{-13}\left(\frac{10^4K}{T}\right)^{3/4}\frac{cm^3}{s},\quad \Gamma_{12}\approx 0.7$$

((Black, 1981, Rauch et al. 1997). Finally, for the column density of neutral hydrogen we have

$$N_{HI} = N_0\xi(b)\left(\frac{b_{bg}}{b}\right)^{3/2}\frac{\langle\delta_{bar}\rangle}{\Gamma_{12}}\kappa\zeta^3\Theta_H, \qquad (2.16)$$

$$N_0 = 8.6\cdot 10^{13}cm^{-2},\quad \Theta_H = \frac{\Theta_{bar}^2\tau_z^2}{\Theta_m\nu}.$$

and $\xi(b)$ was introduced by (2.2) and (2.6) or (2.9).

The relation (2.16) links the observed column density of neutral hydrogen and the Doppler parameter with the column density of baryons and dark matter, $\xi(b)$, and the degree of matter compression, $\langle\delta_{bar}\rangle$. The degree of matter compression depends on the entropy of gas and, so, on its evolutionary history that allows us to discriminate between various models of absorbers formation and, in particular, between adiabatic and shock compressions of the gas accumulated within absorbers. Thus, for the adiabatic compression of the gas which is more typical for the formation of smaller DM pancakes

$$\langle\delta_{bar}\rangle = (b/b_{bg})^3,\quad N_{HI}\propto\xi(b)b^{3/2}. \qquad (2.17)$$

On the other hand, to describe formation of rich pancakes we can use the function $\xi(b)$ (2.6) or (2.9). In this cases we have

$$N_{HI}\approx 0.3N_0\frac{\sqrt{\eta}}{1+\sqrt{1+\eta^2}}\frac{\langle\delta_{bar}\rangle}{\Gamma_{12}}\kappa\zeta^{21/4}\Theta_H, \qquad (2.18)$$

$$N_{HI}\approx 0.1N_0\epsilon^{-3/2}\frac{\langle\delta_{bar}\rangle}{\Gamma_{12}}\kappa\zeta^{21/4}\Theta_H, \qquad (2.19)$$

for unrelaxed and relaxed absorbers, respectively. In both cases the expected correlation between $N_{HI}/\langle\delta_{bar}\rangle$ and b is negligible and $N_{HI}\propto\langle\delta_{bar}\rangle$. For such pancakes the overdensity δ_{DM} obtained in Sec. 2.2.1 is not a good parameter because the evolutionary histories and, so, degrees of compression of DM and gaseous components are certainly different.

As seen from (2.18) & (2.19), at redshifts $z\geq 3$, $\zeta\geq 1$ the discussed approach can be applied mainly to rich absorbers with $N_{HI}\geq 10^{13}\text{cm}^{-2}$. For smaller redshifts, $\zeta\leq 1$, this model can also describe the properties and evolution of some fraction of poor absorbers with $N_{HI}\leq 10^{13}\text{cm}^{-2}$ connected with DM pancakes. The range of application of this model increases for $\Gamma_{12}\geq 1$, and depends on the local factors which can change the parameter Θ_H.

Relations (2.17) and (2.18) allow us to estimate the compression factor, $\kappa\langle\delta_{bar}\rangle\Gamma_{12}^{-1}$ and the entropy of gas accumulated by absorbers. Two functions

$$F_S = (T/T_{bg})\delta_{bar}^{-2/3} \propto b^2(\Gamma_{12}/\kappa)^{2/3}, \quad \Sigma = \ln F_S, \qquad (2.20)$$

measure this entropy relatively to the entropy assumed for the homogeneous intergalactic gas (2.13). These functions also depend on the photoionization rate, Γ_γ, and the unknown distribution of neutral hydrogen across absorbers, described by the factor κ.

2.4.3 *Adiabatic compression of gas.*

The velocity of infalling gas (2.3) can be rewritten more transparently as

$$\langle v_{inf}\rangle \approx 62.5km/s\ \xi\tau_z^2\zeta^{-3/2}\Theta_m^{-1/2}, \qquad (2.21)$$

$$\sigma_{inf} \approx 47km/s\ \xi^{1/2}\tau_z^2\zeta^{-3/2}\Theta_m^{-1/2}, \qquad (2.22)$$

and for poor pancakes with $\xi \leq 0.25\zeta^{3/2}$, when $\langle v_{inf}\rangle \leq b_{bg} \approx 16km/s$, the formation of DM pancakes is accompanied by the adiabatic compression of gas. As seen from Eq. (2.17), in this case

$$\xi(b) \propto N_{HI}b^{-3/2} \ll 1,$$

and Eq. (2.2) shows that the homogeneous distribution can be expected for both ξ and $N_{HI}b^{-3/2}$.

This conclusion can be, in principle, tested using the observed sample of absorbers. Unfortunately, the available sample of weaker Ly-α lines is poor and incomplete and cannot provide the statistics required for such test. Moreover, such absorbers are more strongly influenced by random local factors that also can destroy the expected correlation between b and N_{HI}. On the other hand, the same factors can generate the local shock waves without any connection with the evolution of dark matter. Moreover, this sample is complex and it also includes absorbers which are not a byproduct of the process of DM structure formation.

2.4.4 *Shock compression of gas.*

Under the shock compression the gas density increases not more than 4 times while the Doppler parameter increases proportionally to v_{inf}. Simple estimates similar to that given in Zel'dovich & Novikov (1983) for "Zel'dovich pancakes" and Meiksin (1994) for the collapse of ionized gas into slabs show, however, that even for the strong compression of homogeneously distributed gas the smooth profile of $v_{inf} \propto \xi$ (2.21) leads to strong adiabatic compression of the gas before formation of shock waves (see, e.g., Nath 1997).

For the observed range of Doppler parameters the most plausible scenario of gas evolution is shock compression of the gas already accumulated within the DM confined pancakes and clouds ('grain' model). This process is typical for the merging of earlier formed structure elements. Such matter distribution reduces the adiabatic compression of the gas during the stage when clouds approach each other. The shock wave is formed at the moment of merging of clouds and only shock compression occurs. This process results in an essential increase of the entropy because of the limited growth of density and larger growth of the temperature $T \propto v_{inf}^2$.

This scenario can be realized if a high matter concentration within DM confined structure elements has occurred before creation of observed absorbers. Such strong matter concentration within clouds, similar in some respects to that considered in the 'mini-halo' model (Rees 1986, Miralda-Escude & Rees 1993), is consistent with the theoretical expectations (DD99) because, for the CDM-like transfer function and Harrison – Zel'dovich primordial power spectrum, the majority of matter should be accumulated by low mass clouds with $M_{DM} \sim 10^7 M_\odot(\Omega_m h^2)^{-2}$ already at redshifts $z \geq 5$. This conclusion is consistent with simulations (see, e.g., Zhang et al. 1998) which demonstrate that only $\sim 5\%$ of baryons remains in a smoothly distributed component.

The analysis of observational data (see below) shows that for observed samples there is a strong correlation between the entropy and the Doppler parameter, while b and N_{HI} are practically not correlated. For richer absorbers, with $N_{HI} \geq 10^{13}cm^{-2}$, the entropy distribution can be approximated as $F_S \propto b^2$ what agrees well with this model of shock heating of gas with strongly nonhomogeneous distribution.

The entropy, Σ, given by (2.20) is an additive function which accumulates the successive contributions of shock and bulk heating during all evolutionary history of a given gaseous element. If the shock heating of gas dominates, then the growth of entropy, Σ, can be described as a random process – similar to the Brownian motion – with a successive uncorrelated jumps of entropy at each step. This means that the expected PDF of the entropy, Σ, should be similar to Gaussian.

For the samples of poorer absorbers with $N_{HI} \leq 10^{13}cm^{-2}$ there are both substantial correlations between b and N_{HI} and between the entropy and the Doppler parameter. This fact indicates the complex character of such absorbers. If they can be associated with pancake-like DM elements then for some fraction of such absorbers the adiabatic compression or bulk heating could be significant, while some of them could be formed due to expansion of richer earlier formed pancakes. Some fraction of such absorbers can be also related to artificial pancakes discussed by McGill (1990) and Levshakov & Kegel (1996, 1997) and to absorbers situated within "minivoids" what increases uncertainty in their discrimination.

2.4.5 *Bulk heating and cooling of the gas.*

The bulk heating and cooling of the compressed gas can be also essential for the evolution of properties of absorbers. The main factor is the random spatial variation of the spectrum of ionizing UV radiation field generated by local sources (Zuo 1992, Fardal & Shull 1993). The action of this factor can be characterized by the mean energy injected at photoionization, $T_\gamma \approx (5 - 10)\cdot 10^4 K$ for suitable spectra of UV radiation (Black 1981). In extremal cases such variations are observed as a proximity effect (Bajtlik, Duncan & Ostriker 1988). In the model of DM confined absorbers discussed here, when the gas temperature is given by the gravitational potential of DM component, the bulk heating changes the density and entropy of compressed gas.

The influence of the bulk heating can be enhanced by the pancake disruption due to the clustering of both DM and baryonic components. This process is usually accompanied by adiabatic reduction of temperature in expanded regions when the role of the bulk heating becomes more important. As is shown in Appendix B, in the general case, for redshift dependent $T(z)$ & $T_\gamma(z)$ we have

$$F_S^{3/2}(z) = F_S^{3/2}(z_f) + \alpha_s \int_z^{z_f} dx \frac{H_0}{H(x)} \frac{T_\gamma(x) - T(x)}{(1+x)T_{bg}},$$

$$\alpha_s = 1.5h^{-1}\zeta^3\Theta_{bar}, \qquad (2.23)$$

where the entropy function F_S was introduced by (2.20) and z_f is the redshift of pancake formation. For example, under condition of slow variation of the DM distribution when $T(z) \approx$ const. and for $T_\gamma \approx$ const. we have

$$F_S^{3/2}(z) = F_S^{3/2}(z_f) + \alpha_s\ H_0[t(z) - t(z_f)]\frac{T_\gamma - T}{T_{bg}},$$

$$t(z) = \int_z^\infty \frac{dx}{H(x)(1+x)},$$

that indicates the slow growth of entropy and drop of the density of absorbers.

At higher redshifts the proper separation of structure elements is about D_{sep} ∼0.5 – $1h^{-1}$Mpc that is comparable with sizes of galactic halos observed at small redshifts ∼ $0.2h^{-1}$Mpc (see, e.g., Bahcall et al. 1996). This means that the evolution of structure elements at such redshifts could be interdependent and activities in galaxies can increase the gas entropy within nearby pancakes. Analysis of Cen & Ostriker (1993) shows that the input of explosive energy can be essential in the vicinity of virialized objects. In this case the gas overdensity decreases in proportion to the injected energy and the additional correlations between the Doppler parameter and column density of neutral hydrogen do not appear. The observations of metal systems together with relatively weak Ly-α lines shows that sometimes the influence of such heating can be important.

2.4.6 Evolution of hydrogen column density

The observed column density of absorbers is changed due to irreversible processes such as shocks and bulk heating, and due to adiabatic expansion and/or compression of pancakes caused by the transversal motions of DM component (DD99, Paper I). The heating of the gas does not distort the DM distribution and the ionization equilibrium and, as was discussed in Sec. 2.4.5, also the relatively slow decrease of $N_{HI} \propto \langle\delta_{bar}^2\rangle$. The adiabatic compression and expansion of DM and gaseous components also does not distort the ionization equilibrium, but changes the observed column density $N_{HI} \propto b^{9/2}$, and can lead to the appearance of rare absorbers with larger and smaller N_{HI} and b.

These simple arguments demonstrate the important role of adiabatic evolution of DM pancakes for the formation of observed sample of absorbers. Together with the merging these processes lead to the fast evolution of linear density of absorbers discussed in Paper I and are essential for the formation of both rare absorbers, with larger N_{HI}, and weaker absorbers.

2.5 Theoretical expectations

The previous consideration can be shortly summarized as follows:

(i) For the DM confined absorbers the observed Doppler parameter, b, is closely linked to the column density of DM pancakes, q, and the expected PDFs of the b parameter, (2.7) and (2.9), are similar to the gamma-distribution. The density field can be described as a set of discrete pancakes with masses $\propto q(b)$.

(ii) For such absorbers only weak correlation between the Doppler parameter, b, and the column density of neutral hydrogen, N_{HI}, is expected under the assumption of ionization equilibrium.

(iii) The same factors result in the strong correlation between the entropy of compressed gas and the Doppler parameter. Due to merging and shock heating the gas entropy increases. This growth can be described as a random process with the function $\Sigma = \ln F_S$ increasing discontinuously with jumps depending on the mass of merging pancakes. The possible bulk heating caused by the local sources results also in random jumps of entropy. More detailed description of entropy evolution can be obtained on the basis of Fokker-Plank equation that implies however more detailed description of the pancake evolution and assumptions about the local activity of galaxies. In any case approximately Gaussian distribution of Σ can be expected.

(iv) As is seen from equations (2.18), (2.19) & (2.20) for such pancakes the approximately Gaussian PDFs are also expected for $\log\delta_{bar}$ and $\log N_{HI}$.

(v) The adiabatic compression of the gas dominates for poorer DM pancakes with $N_{HI} \leq 10^{13}cm^{-2}$ and creates much stronger correlation between N_{HI} and b. This correlation can be, however, partly destroyed by the action of local random factors. Formation of such absorbers is often not accompanied by formation of DM structure elements.

As is seen from (2.16) and (2.20) the *observed* estimates of entropy, Σ, and the column density, N_{HI}, depend on the intensity of UV ionizing radiation (factor Γ_{12}). This means that local variations of the ionizing rate introduce the essential random factor in observational estimates of both entropy and column density. The rapid growth of observed number of galaxies at $z \leq 3$ (Steidel et al. 1998; Giavalisco et al. 1998) correlates well with the observed rapid evolution of linear density of absorbers, n_{abs}, (Paper I) what points toward galaxies as the essential factor of observed evolution of absorbers.

2.6 Characteristics of absorbers in simulations

High resolution simulations of dynamical and thermal evolution of gaseous component cited above give us valuable examples of absorbers formed at redshifts $z \leq$5 and allow to clarify many peculiarities and properties of these processes. In particular, they confirm the existence of high density clumps, filamentary and sheet-like components of structure at high redshifts and demonstrate that these elements accumulate up to 95% of baryons and reproduce well the main observed characteristics of absorbers. They confirm the domination of adiabatic compression of baryonic component in less massive pancakes and show that some fraction of weaker absorbers can be identified with underdense structures (Bi & Davidsen 1997; Zhang et al. 1998; Davé et al. 1999). List of these examples can be essentially extended.

At the same time, the abilities of simulations in statistical description of absorbers evolution are limited as the main simulations are performed with small box sizes (∼10 Mpc) that is comparable with the mean separation of galaxy filaments at small redshifts, and is smaller then the mean separation of richer galaxy walls ($\sim 40 - 60h^{-1}$Mpc) and even their Lagrangian size ($\sim 15 - 20h^{-1}$Mpc). The small box sizes restrict the important influence of large scale perturbations on the evolution of small scale structure and does not allow to establish direct connection of structure at high redshifts with galaxy distribution observed at small redshifts.

Moreover, some results obtained in simulations should be explained in more details. Thus, for example, in all papers the very important problem of quantitative characteristics of absorbers morphology is not discussed and the merging of pancakes and filaments is not considered. Such merging is certainly responsible for the formation of observed galactic walls and was discussed in DD99, DDMT, Paper I and in Sec. 2.2 & 2.3 above as one of the main factors of absorbers evolution. Its action can be easily traced using the analysis of entropy of compressed gas. The distribution function of temperature (Fig. 10 in Zhang et al. 1998) is quite different from the observed distribution of Doppler parameter. The strong contribution of macroscopic motions in simulated Doppler parameter plotted in Fig. 13 increases it about of 2 – 5 times with respect to the thermal value what probably implies the supersonic character of typical macroscopic motions within simulated structure elements. In contrast, the analysis of DM evolution in large boxes demonstrates an approximate isotropy of subsonic velocity dispersion within DM structure elements at small redshifts, and its close connection with the measured richness of such element (DMRT, DDMT). The physical reasons of the power distribution of N_{HI} plotted in Fig. 15 of the same paper, in the range of 5 orders of magnitude, are also not explained.

Even these examples demonstrate an essential scatter of some quantitative characteristics of structure obtained with different codes and parameters of simulations (see also discussion in Melotte et al. 1997; Splinter et al. 1998; Theuns et al. 1999). They show also the usefulness of more detailed comparisons and tests of consistency of results obtained with different approaches and box sizes, and based on larger set of characteristics. Bearing in mind the relatively small number of such complicated simulations, these differences, list of which can also be continued, seem to be natural.

3 THE DATABASE.

The present analysis is based on the spectra available in the literature. The list of the used sources of data is given in Table 1. As was discussed in Paper I absorbers with $b \geq$ 17km/s or $\log(N_{HI}) \leq 14$ can be probably related to the sheet-like component of structure. In spite of statistical character of such discrimination it allows us to obtain more homogeneous sample of sheet-like absorbers used for comparison with theoretical expectations. The list of available Ly-α lines was arranged into three samples. Two of them, Q_{12} and Q_{14} include 2073 and 2378 lines from the first 12 and all 14 spectra, respectively, under conditions that $b \geq 17$km/s and $10^{13}cm^{-2} \leq N_{HI} \leq 10^{14}cm^{-2}$. First condition allows us to discriminate and to exclude absorbers which could be possibly formed due to the adiabatic compression.

Table 1. QSO spectra from the literature

Name	z_{em}	z_{min}	z_{max}	FWHM km/s	No of lines
$0000-260^1$	4.11	3.4	4.1	7	431
$0014+813^2$	3.41	2.7	3.2	8	262
$0956+122^2$	3.30	2.6	3.1	8	256
$0302-003^2$	3.29	2.6	3.1	8	266
$0636+680^2$	3.17	2.5	3.0	8	313
$1946+766^3$	3.02	2.4	3.0	8	461
$0055-259^4$	3.66	2.9	3.1	14	313
$2126-158^5$	3.26	2.9	3.2	11	130
$1700+642^6$	2.72	2.1	2.7	15	85
$1225+317^7$	2.20	1.7	2.2	18	159
$1101-264^8$	2.15	1.8	2.1	9	84
$1331+170^9$	2.10	1.7	2.1	18	69
$1033-033^{10}$	4.50	3.7	4.4	18	299
$2206-199^{11}$	2.56	2.1	2.6	11	101

1. Lu et al. (1996), 2. Hu et al., (1995), 3. Kirkman & Tytler (1997), 4. Cristiani et al. (1995), 5. Giallongo et al. (1993), 6. Rodriguez et al. (1995), 7. Khare et al. (1997), 8. Carswell et al. (1991), 9. Kulkarni et al. (1996), 10. Williger et al. (1994), 11. Rauch et al. (1993),

The sample Q_{0612} contains 469 lines with $N_{HI} \leq 10^{13}cm^{-2}$ and $b \leq 30$km/s from the first 6 QSOs. This sample is incomplete as was discussed by Hu et al. (1995). It can be used for the estimates of properties of poor absorbers.

The line distribution over redshift is nonhomogeneous and the majority of lines are concentrated at $z \approx 3$. The distribution of absorbers at $z \geq 3.2$ is based mainly on the spectrum of QSO 0000-260 (Lu et al. 1996) and here the line statistics is insufficient. The inclusion of the spectrum of QSO 1033-033 extends the redshift interval up to $z \approx 4.4$, but cannot eliminate small representativity of the sample at such redshifts.

4 STATISTICAL CHARACTERISTICS OF ABSORBERS

Some statistical characteristics of absorbers were found for samples Q_{12} and Q_{14} for four ranges of redshifts. Main results are listed in Table 2 and plotted in Figs. 1 – 4.

4.1 Distribution of observed Doppler parameter, b, and DM column density, q

As was discussed in Sec. 2.2, the observed distribution of Doppler parameter, b, can be interpreted as the distribution of DM column density of absorbers. To check this hypothesis the observed distribution of $b/\langle b\rangle$ was fitted to the two parameters function similar to (2.6) & (2.7)

$$N_b = c_1 \mathrm{erf}(\sqrt{y}) \frac{\sqrt{2+y}}{1+y} \exp(-y), \tag{4.1}$$

Table 2. Main parameters of Ly-α absorbers.

	z_{min}	z_{max}	N_{line}	ζ	$\langle b\rangle$ km/s	$\langle q\rangle$	c_2	τ_b	r_{bH}	$\langle F_S\rangle$	p_{bs}	σ_S
					Q_{12}							
a	1.7	4.1	2073	0.98	36.9	0.2	1.6	0.17	0.04	4.8	1.89	0.9
b	2.0	3.0	1118	0.92	37.6	0.2	1.5	0.17	-0.04	5.0	2.14	0.9
c	2.5	3.5	1392	0.98	36.8	0.2	1.9	0.18	0.02	4.9	2.05	0.9
d	3.0	4.1	813	1.10	36.0	0.2	2.0	0.19	0.16	4.8	1.59	0.8
					Q_{14}							
	1.7	4.4	2378	1.00	38.2	0.2	1.9	0.16	0.11	6.1	1.91	0.8
	2.0	3.0	1190	0.92	37.3	0.2	1.6	0.17	-0.02	4.8	2.10	0.8
	2.5	3.5	1403	0.98	36.8	0.2	1.7	0.17	-0.02	4.6	2.05	0.8
	3.0	4.4	1046	1.11	39.5	0.3	1.8	0.21	0.23	5.4	1.86	0.8

The correlation coefficient r_{bH}, exponent p_{bs} and the entropy dispersion σ_S are introduced in Secs. 4.3 and 4.2, respectively.

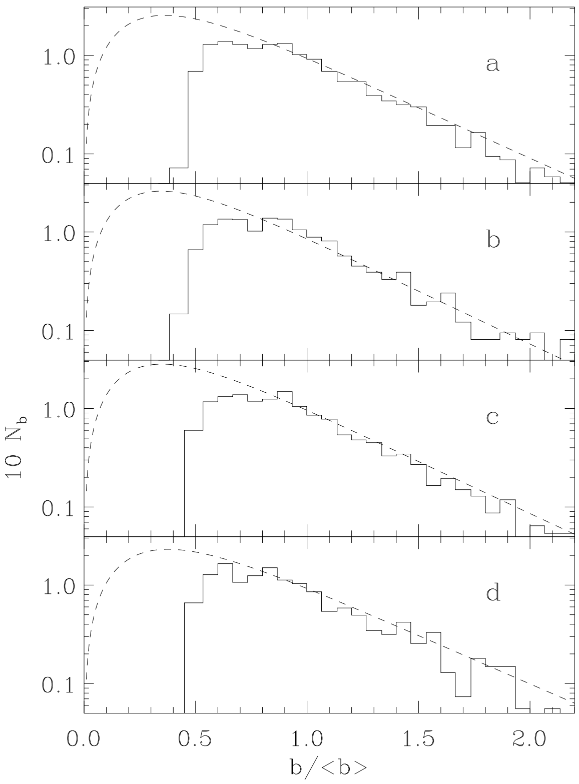

Figure 1. The distributions of Doppler parameter, $b/\langle b\rangle$, for the sample Q_{12} of Ly-α lines for different redshifts. The best fits (4.1) are plotted by dashed lines. The main parameters of subsamples are listed in Table 2.

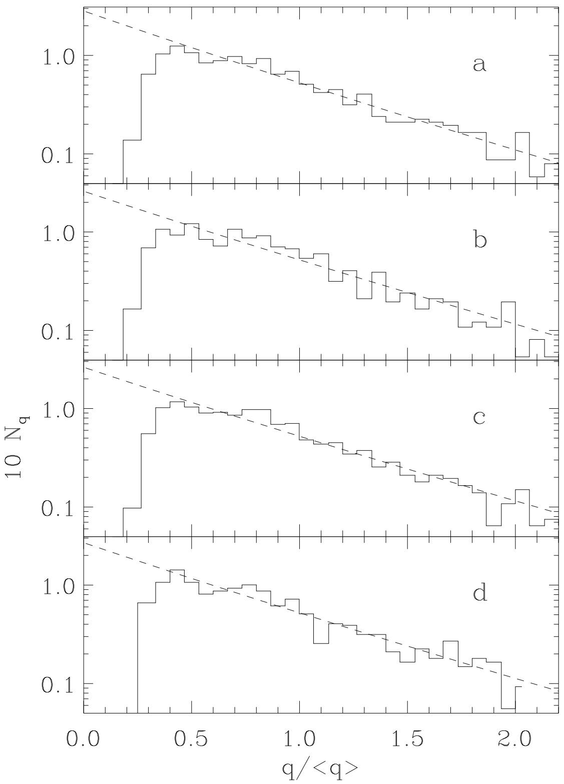

Figure 2. The distributions of DM column density, $q/\langle q\rangle$, for the sample Q_{12} of Ly-α lines for different redshifts. The best fits (2.2) are plotted by dashed lines. The main parameters of subsamples are listed in Table 2.

$$y=\sqrt{1+c_2^2b^2/\langle b\rangle^2}-1=\frac{c_2^2b^2/\langle b\rangle^2}{1+\sqrt{1+c_2^2b^2/\langle b\rangle^2}},$$

for both samples and four different ranges of redshifts. For each absorber the dimensionless column density of DM component, q, was found using Eq. (2.6) and its distribution was fitted to a two parametric function

$$N_q\approx c_3e^{-y}\,\frac{\mathrm{erf}(\sqrt{y})}{\sqrt{y}},\quad y=c_4q/\langle q\rangle. \qquad (4.2)$$

The main results are listed in Table 2 and plotted in Figs. 1 & 2.

The observed properties of the Doppler parameter, b, are found to be surprisingly stable and independent of samples or redshift ranges. In all cases we have

$$\langle b\rangle=37km/s,\quad \sigma_b=0.55\langle b\rangle. \qquad (4.3)$$

The functions (4.1) & (4.2) fit well the observed $b\&q$ distributions for all samples under consideration. Fit parameters $c_1\&c_2$ and $c_3\&c_4$ describe the cutoff in observed PDFs at $b\approx 0.5\langle b\rangle$. This cutoff naturally appears for the Doppler parameter of gaseous component as in both samples, Q_{12} & Q_{14}, absorbers with $b\leq 17km/s\approx 0.5\langle b\rangle$ were excluded from the analysis. This cutoff increases the observed $\langle b\rangle$ and $\langle q\rangle$ by the factor of c_2 and c_4, respectively, in comparison with theoretical expectations for the velocity

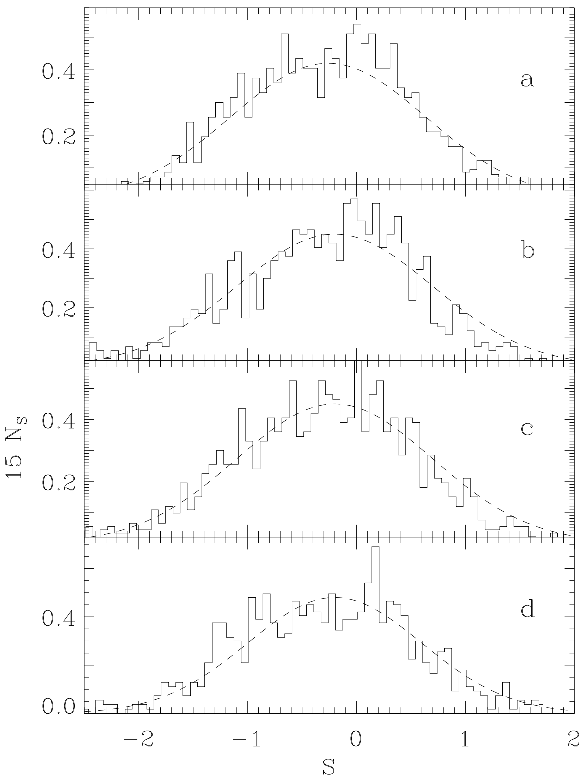

Figure 3. The distribution function of absorbers 'entropy', S, for the sample Q_{12} for four different redshifts. The best Gaussian fits are shown by dashed lines.

and column density of DM component. Some deficit of absorbers with larger $b \geq (2-2.5)\langle b\rangle$ is seen in Fig. 1. For the PDF (4.1) the expected value is $\sigma_b = 0.7\langle b\rangle$. The difference between observed and expected σ_b is also explained by the same cutoff and for $y \geq 0.5$, the expected $\sigma_b = 0.6\langle b\rangle$ is practically identical to (4.3).

The fitting parameters $c_2\&c_4$ allow us to correct measured $\langle b\rangle$ and $\langle q\rangle$ for the cutoff at $b \approx 0.5\langle b\rangle$ and to estimate the amplitude and time scale of the DM structure evolution, τ, as given by (2.2) and (2.6):

$$\tau_b = (1+z)\tau = (1+z)\sqrt{\frac{\langle q\rangle}{6.55c_4}}$$

$$= (1+z)\sqrt{\frac{\langle b\rangle}{720km/s\ c_2}}\zeta^{3/4}\Theta_m^{1/4} \approx (0.17\pm 0.1). \qquad (4.4)$$

c_2 and τ_b listed in Table 2 are found to be weakly dependent on redshift z and on subsamples used. This value τ_b is roughly consistent with the values $(1+z)\tau \sim 0.2-0.4$ expected for low density cosmological models (Appendix A).

We can also estimate the typical proper thickness of DM absorbers, h_{DM}, which is linked with τ by Eq. (2.3), we have

$$\langle h_{DM}\rangle \approx \frac{8}{\sqrt{\pi}} l_0 \frac{\tau^2}{1+z} \sim \frac{130\text{kpc}}{\Theta_m\zeta^3}\left(\frac{\tau_b}{0.17}\right)^2. \qquad (4.5)$$

This value is approximately consistent with sizes found by Dinshaw et al. (1995) and is similar to the measured sizes of galactic halos at small redshifts (Lanzetta et al. 1995; Bahcall et al. 1996) and to results obtained in Paper I. We cannot obtain reasonable estimates of the size, $\langle\Delta r\rangle$, and overdensity $\langle\delta_{bar}\rangle$, of gaseous halo because they depend on the unknown parameter κ introduced in (2.14) which characterizes the distribution of neutral hydrogen across absorber.

4.2 Entropy of absorbers.

The observed characteristics of the entropy described by the functions F_S and Σ (2.20) were found for the same subsamples of absorbers and the main results are plotted in Figs. 3 and listed in Table 2. The function F_S can be fitted to the expression

$$F_S = \langle F_S\rangle \left(\frac{b}{\langle b\rangle}\right)^{p_{bs}} \exp(S),\ S = \Sigma - p_{bs} ln\left(\frac{b}{\langle b\rangle}\right), \quad (4.6)$$

which discriminates between the regular variations of the entropy described by the first terms in (4.6), and the integral action of random factors described by the function S. The PDF of S plotted in Figs 3 is fitted to Gaussian functions with σ_S listed in Table 2. It is found to be sufficiently stable and weakly sample depended. At larger S the deficit of absorbers with higher entropy is seen as an asymmetric shape of PDF. It can be caused by the deficit of observed absorbers with larger b and smaller N_{HI}. Estimates of $\langle F_S\rangle$ listed in Table 2 show that the entropy of absorbers with larger $b \geq (4-5)\langle b\rangle$ is similar to the entropy of gas accumulated by clusters of galaxies as is given in Sec. 2.4.1.

The value $p_{bs} \approx 2$ shows that merging of pancakes is the main factor of entropy evolution. It shows also that among pancake merging there is one which provides the main jump in both the Doppler parameter and entropy and their correlation. The impact of smaller jumps in the course of the merging of pancakes, random local variations of ionizing UV radiation, a possible bulk heating and other random factors is well described by the Gaussian distribution of S-function. It agrees well with negligible correlation of measured N_{HI} and b, since the correlation coefficient $r_{bH} \leq 0.1$.

The small range of observed redshifts, $0.8 \leq \zeta \leq 1.2$, does not allow more detailed analysis of possible variations of the mean entropy with z. Nonetheless, the weak decrease of p_{bs} and corresponding growth of r_{bH} at $z \geq 3$ shows that for larger z the merging of pancakes could be accompanied by other irreversible processes and/or by adiabatic gas compression.

4.3 Observed distribution of column density of HI.

One of the most enigmatic feature of the distribution of observed column density of neutral hydrogen is that it can be approximated by a single power law with a power index $\beta_H = 1.5 \pm 0.05$ in the range $10^{13}cm^{-2} < N_{HI} < 10^{22}cm^{-2}$ (see, e.g., Tytler 1987, Hu et al. 1995, Kim et al. 1997). For smaller N_{HI} the deviations from the fit are usually assigned to the incompleteness of samples. It is interesting that similar power distribution was found (but not explained) in simulations as well (Zhang et al. 1997, 1998)

In the considered model of absorbers, when the gas temperature and the Doppler parameter, b, are hardly linked with characteristics of DM distribution, the well known negligible correlation of N_{HI} and b indicates the weak connection of N_{HI} with the properties of DM component of absorbers, such as, in particular, the DM surface density of

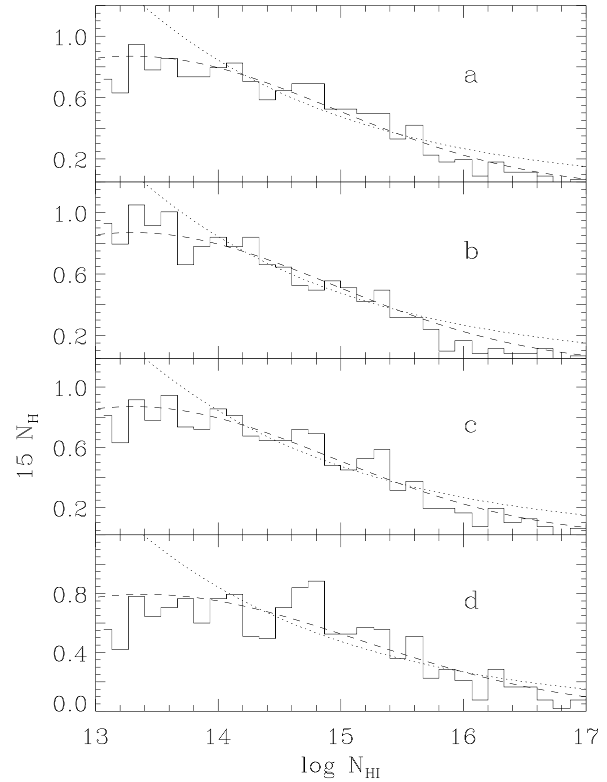

Figure 4. The distribution function of $\log N_{HI}$ for the sample Q_{12} for four ranges of redshifts. Parameters of samples and fitting parameters are listed in Table 2. The best fits (4.8) and (4.9) are plotted by dashed and dotted lines, respectively.

pancake, q. For samples under consideration the correlation coefficient

$$r_{bH} = \frac{\langle logN_{HI} * log\ b\rangle - \langle logN_{HI}\rangle\langle log\ b\rangle}{\sigma_{logN_{HI}}\sigma_{log\ b}}, \quad (4.7)$$

was estimated directly using measured b and $logN_{HI}$ and in all the cases r_{bH} $\leq$0.1 were found (Table 2). For the DM dominated absorbers the column densities of baryonic component and, therefore, also N_{HI} depend mainly on the entropy of gas, F_S or Σ, which accumulates the contribution of irreversible processes during all evolutionary history of the compressed gas. The action of this factor disconnects the surface densities of baryonic and DM components, N_{HI} and $q\&b$. Essential variations of the entropy implies essential variations of observed N_{HI} even for the same temperature, b, and DM surface density, q. This means that it is difficult, if not impossible, to explain this joint power distribution in such a wide range of column density.

The negligible correlation between the observed b and N_{HI} implies also that

$$N_{HI} \propto \langle\delta_{bar}\rangle \propto (F_S/b^2)^{-2/3}, \quad \log N_{HI} \approx -\frac{2}{3}S + \text{const.}$$

This means that at least for the considered subsample of pancake-like absorbers the PDF for observed N_{HI} should be similar to PDF of the function S, discussed in previous Subsec. Therefore, the expected PDF of $\log(N_{HI}/N_m)$, $N_m = 10^{13}cm^{-2}$, is Gaussian and can be written as

$$N_H = N_0 \exp\left[-\frac{1}{2\sigma_H^2}\log^2\left(\frac{N_{HI}}{N_m}\right)\right]. \quad (4.8)$$

The distribution function of $\log(N_{HI})$ is plotted in Fig. 4 for four redshift intervals, for the sample of 12 QSO and for all observed lines, with $N_{HI} \geq 10^{13}cm^{-2}$. The physical model of absorbers evolution introduced in Secs. 2.2 and 2.4 applies only to absorbers with $N_{HI} \leq 10^{14}cm^{-2}$. The distribution of stronger absorbers, which are probably linked with filaments and high density clumps, should be discussed in a context of spatial distribution and evolution of these components of structure. The statistics of absorbers with $N_{HI} \geq 10^{14}cm^{-2}$ is limited, and the right part of Figs. 4 is rather illustrative but, even so, these Figs. demonstrate that the relation (4.8) also approximately fits the observed distribution of N_{HI} up to $N_{HI} \sim 10^{17}cm^{-2}$.

The power distribution of N_{HI} corresponds to the exponential distribution of $log(N_{HI})$ and can be written as

$$N_H \propto \exp\left[2.30(1-\beta_H)\log\left(\frac{N_{HI}}{N_m}\right)\right]. \quad (4.9)$$

This fit is plotted in Figs. 4 by dotted lines for $\beta_H \approx 1.5$ (Hu et al. 1995; Kim et al. 1997). It agrees with the observed PDF N_H for larger $log(N_{HI})$ but predicts some excess of weaker lines.

These results show that the problem deserves further investigation in a wider range of redshifts with a more representative sample of absorption lines.

5 PROPERTIES OF WEAKER ABSORBERS

The sample of observed weaker absorbers with $N_{HI} \leq 10^{13}cm^{-2}$ and $b \leq 30$km/s is incomplete and composed of only 469 lines in 6 QSOs listed in Table 1. This factor as well as the much more complicated composition of this subpopulation indicate illustrative character of our consideration in this subsection.

As was discussed in Sec. 2.2 such absorbers can be created by adiabatic compression of homogeneous gas or the disruption and adiabatic expansion of earlier formed rich pancakes. For the first subpopulation the entropy is not changed and $F_S \approx 1$ can be expected. For such pancakes b and F_S are evidently uncorrelated, but significant correlation between N_{HI} and b can be expected. For the second subpopulation $F_S \geq 1$ and, as before, it correlates with b, but N_{HI} and b are only weakly correlated. Moreover, for such absorbers the contribution of artificial pancakes discussed in McGill (1990) and Levshakov & Kegel (1996, 1997) and absorbers formed within "minivoids" (Zhang et al. 1998) can be more significant.

This means that the population of weaker absorbers consists of objects with different evolutionary history, and the available observational data do not allow us to discriminate between these subpopulations. So, we have to restrict our consideration to the analysis of PDF for the column density of DM component $q \propto N_{HI}b^{-3/2}$, as was described in Sec. 2.4.3.

This PDF, N_q, is plotted in Fig. 5. As was expected for smaller q, $N_q \approx$ const. especially at larger redshifts $z \geq 3$. The significant correlation between $\log N_{HI}$ and $\log b$, since $r_{bH} \approx 0.4$, agrees also with the probable substantial contribution of adiabatically compressed subpopulation of weaker absorbers. The 'tail' of absorbers with larger $q/\langle q\rangle$ can be associated with the subpopulation of disrupted and/or ex-

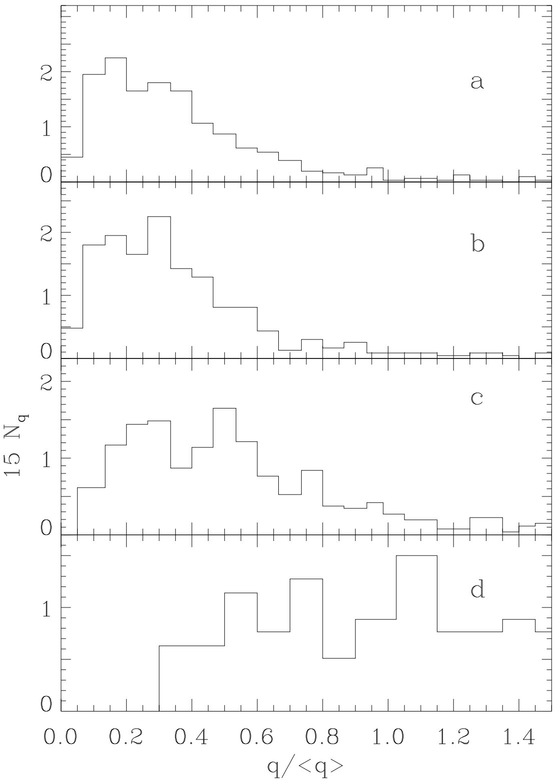

Figure 5. The distributions function of $q \propto N_{HI} b^{-3/2}$ for the sample of weaker absorbers with $N_{HI} \leq 10^{13} cm^{-2}$ and $b \leq 30$ km/s for the same ranges of redshifts.

panded earlier formed richer absorbers. The fraction of such absorbers increases for smaller z.

6 SPATIAL DISTRIBUTION OF ABSORBERS

The observed redshift distribution of absorbers contains significant information about the spatial matter distribution at high redshifts, as suggested in particular by Oort (1981, 1984). The available absorption spectra cover typically the range $D \sim 200 - 300(\Omega_m)^{-1/2}h^{-1}$Mpc, whereas a mean separation of weak absorbers with $N_{HI} \approx 10^{12} cm^{-2}$ is $\sim 1(\Omega_m)^{-1/2}h^{-1}$Mpc. This allows us to analyze both the small and large scale matter distribution.

6.1 Small scale absorber distribution

During last years weak clustering of Ly-α absorbers on small scales ($\Delta v \leq 300$km/s) have been found for a few quasars (Webb 1987; Cristiani et al. 1995; Hu et al. 1995; Ulmer 1996; Fernandes-Soto 1996). For many other objects such clustering is negligible and the absorbers distribution is nearly Poissonian. Stronger small scale correlation, found for metal lines, is naturally explained since several lines can be generated in the same gaseous cloud. At the same time much stronger correlation of galaxies is found both at small and even high redshifts (see, e.g., discussion in Steidel et al. 1998; Governato et al. 1998; Giavalisco et al. 1998)).

This divergence can be naturally explained in the framework of discussed here approach, when absorbers are associated with structure elements – filaments and pancakes – rather then with galaxies. The distribution of structure elements along a random straight line is expected to be Poissonian - like (DD99, DDMT) what is consistent with the observed distribution of filaments and walls at small redshifts (Doroshkevich et al. 1996). In contrast, the point - like high density clumps, which can be associated with 'galaxies', are mainly incorporated into filaments and massive pancakes. Even for randomly distributed filaments and pancakes this concentration introduces some regularity in the spatial distribution of such clumps in comparison with the 3D Poissonian distribution. As was shown by van de Weygaert (1991) and Buryak & Doroshkevich (1996) such point concentration generates the 3D correlation function similar to that observed for galaxies.

Similar situation occurs, for example, for the LCRS, where the usual correlation function of galaxies was found (Tucker et al. 1997). However, for the same observed sample the 1D distribution of both filaments and walls (in radial and transversal directions) were found to be Poissonian – like.

6.2 Large scale modulation of absorbers distribution

The smoothed absorbers distribution can be compared with expectations discussed in Sec. 2.3. Three expressions for DM distribution are examined: 1) as was discussed in Sec. 2.2.2, for relaxed pancakes $q \propto b^{3/2}$ can be expected, 2) if the compressed matter is not completely relaxed, then $q \propto \sqrt{1+\eta^2} - 1$ is more probable, and 3) for comparison with the previous definition, the hypothesis $q \propto N_{HI}$ is also tested. The third expression is correct for weaker absorbers discussed in Sec. 2.4.3 and Sec. 5 and, possibly, can be also applied to high density peaks associated with galaxies but its application to main part of absorbers is in question.

For separate QSO the observed absorbers distribution along a line of sight was averaged with the Gaussian window function and the smoothed density was found as

$$\frac{\rho(x)}{\langle\rho\rangle} = \frac{1}{W_n(x)} \sum_i \frac{q_i}{\langle q\rangle} W(x - y_i), \qquad (6.1)$$

$$W(y-x) = \frac{1}{2\pi r_s} \exp\left(-\frac{(y-x)^2}{2r_s^2}\right), \;\; W_n = \int_0^D dy W(x-y),$$

where $y_i \& q_i$ are coordinates and DM column density of absorber, and W_n is a normalization factor taking into account the finite size of observed spectra. The results obtained for absorbers with $N_{HI} \geq 10^{13} cm^{-2}$ and averaged over 15 r_s, $7.5\Omega_m^{-1/2}h^{-1}\text{Mpc} \leq \; r_s \; \leq 40\Omega_m^{-1/2}h^{-1}$Mpc, are plotted in Fig. 6 together with the dispersions plotted as error bars. Averaging over 12 QSO gives for the three used definitions of q:

$$\langle (1+z)\tau(z)\rangle \approx (0.11 \pm 0.06)(\Theta_m)^{1/4},$$

$$\langle (1+z)\tau(z)\rangle \approx (0.12 \pm 0.05)(\Theta_m)^{1/4}, \qquad (6.2)$$

$$\langle (1+z)\tau(z)\rangle \approx (0.40 \pm 0.22)(\Theta_m)^{1/4}.$$

where, as before, $\Theta_m = 9\Omega_m h^2$. The large scatter of points shows that the used statistics of absorbers is insufficient and

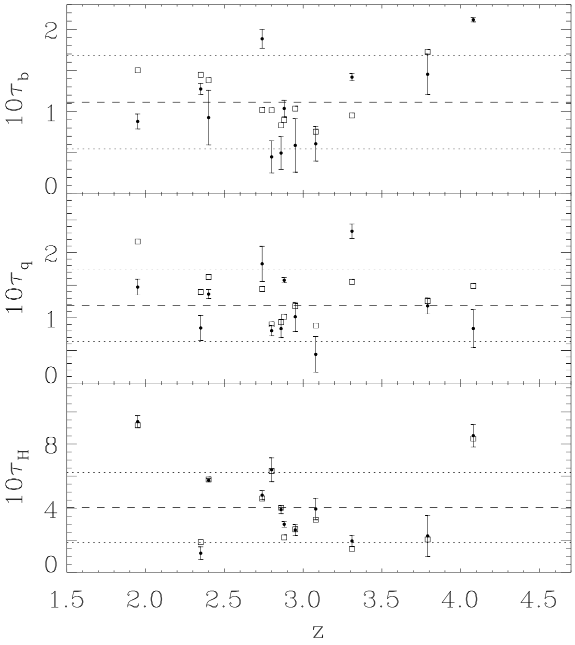

Figure 6. Redshift dependence of the smoothed amplitude, $(1+z)\tau$, vs. z for the sample of 12 QSO. Three definitions of DM density are used: $\rho_{DM} \propto b^{3/2}$ (top panel), $\rho_{DM} \propto (1+\eta^2)^{1/2} - 1$ (middle panel), and $\rho_{DM} \propto N_{HI}$ (bottom panel). Open squares show the same amplitudes obtained for a random redshift distribution of the same absorbers. The mean values are plotted by the dashed lines and the dispersions are shown by dotted lines.

does not allow to obtain reasonable estimates of the amplitude.

These results show that first and second definitions of DM column density lead to similar estimates of τ, whereas the third definition increases it about 4 times.

It is interesting to compare these results with similar estimates obtained for randomly distributed absorbers with the same b and N_{HI}. Results averaged over 100 random realizations are plotted in Fig. 6. For the first and second definitions of DM column density, q, relative to the mean value, does not differ by more than a factor of 2 – 3 and the use of random redshift decreases the dispersion about 2 times. For the third definition variations of q around the mean value are much larger and can exceed a factor of $\sim$ 100. Such a large discrepancy is a result of small fraction of absorbers with largest N_{HI}.

This estimates of $\tau_q \approx \tau_b$ differ by about 2 – 3 times in comparison with the values τ_b obtained in Sec. 4.1. This divergence can be caused by various factors, the most important are probably the small representativity and relatively small size of spectra used, what increases the uncertainty of all estimates for larger smoothing scales.

These results, as well as estimates of τ_b presented in Sec. 4.1, demonstrate the limited abilities of investigations of properties of absorbers with respect to the description of DM distribution. Both theoretical analysis and investigations of simulations (Governato et al. 1998; Jenkins et al. 1998) show that at redshifts $z \sim 3$ high density filaments accumulate main fraction of galaxies and are the most typical and conspicuous structure elements. But such filaments as well as separate galaxies constitute relatively small fraction of the observed absorbers because of their relatively small size, and are represented mainly by the lower density halo. This means that the observed absorbers give us more information about large low density regions of the universe, and estimates of general characteristics of spatial matter distribution derived from such analysis should be essentially corrected.

Results obtained above illustrate the potential and limitations of this approach rather then give the actual estimates of density variations.

7 SUMMARY AND DISCUSSION.

In this paper the observed parameters of Ly-α lines are analyzed and interpreted in the framework of the simple self-consistent theoretical model of the DM structure evolution (DD99). It is shown that the observed evolution of absorbers is sensitive to several random factors and probably does not trace directly the evolution of DM component. Our results show however that some essential observed characteristics of absorbers can be reasonably described even by the statistical model considered here.

The main results of our analysis can be summarized as follows:

(i) The basic observed properties of Ly-α absorbers are satisfactorily described by the discussed statistical model of DM confined structure elements.

(ii) The observed characteristics of Doppler parameter, b, could be linked to the column density of accompanied DM structure elements. It allows us to explain the observed distribution of Doppler parameter which is consistent with the Gaussian distribution of initial perturbations. The measured amplitude of perturbations, τ_b, as given by (4.4), is consistent with that is expected for lower density cosmological models.

(iii) The existence of observed galaxy and simulated DM walls as well as the theoretical arguments demonstrate that the merging of structure elements is one of the most important factors of structure evolution. The observed characteristics of entropy, F_S & Σ, confirm that such a merging can be also considered as probably the main factor of absorbers evolution at redshifts $z \geq 2$.

(iv) For the main fraction of absorbers, the weak correlation of column density, N_{HI}, with Doppler parameter, b, can be reasonably explained by the influence of variations of entropy of compressed gas. The smooth observed distribution of stronger absorbers, with $N_{HI} \geq 10^{14} cm^{-2}$, remains in question and must be investigated, first of all, with larger simulations.

(v) The redshift distribution of absorbers does not repeat the spatial distribution of galaxies and characterizes mainly the matter distribution within larger lower density regions. This makes it difficult to reconstruct the spatial DM distribution from the redshift distribution of absorbers.

The main statistical characteristics of absorbers distribution discussed above coincide with published estimates (see, e.g., Hu et al., 1995; Cristiani 1995, 1996; Kim et al. 1997). They are roughly consistent with the expected evolution of DM structure and can be, in principle, used to test and to discriminate different models of structure evolution. At redshifts $z \geq 3.5$ the Doppler parameter and the mean linear number density of stronger absorbers are more sensitive to the influence of the initial power spectrum of perturbations and to the basic parameters of cosmological model.

The characteristics of DM structure elements discussed in Sec. 2.2 and 4.1 were tested against simulated DM distribution at z=0 (DD99, DMRT, DDMT). The precision reached was $\sim 10\%$. Further application of these methods to broader set of simulations at high redshifts will help to estimate the unknown numerical factors and to improve the proposed here description. The discussed model of structure evolution is limited and cannot yet describe, for example, the structure disruption. It should be improved at least in this respect.

The available database cannot yet provide a precision required for the reliable discrimination of models of structure formation. Now the observational data are concentrated mainly in the narrow range of redshifts $2.2 < z < 3.5$ and therefore the quantitative description of absorbers evolution is difficult. The wider range of observed redshifts is required to improve the description and to obtain more detailed and reliable information about the structure evolution and physical processes at high redshifts.

Acknowledgments

This paper was supported in part by Denmark's Grundforskningsfond through its support for an establishment of Theoretical Astrophysics Center, grant INTAS-93-68 and by the Polish State Committee for Scientific Research grant Nr. 2-P03D-014-17. AGD and VIT also wish to acknowledge support from the Center of Cosmo-Particle Physics, Moscow. Furthermore, we wish to thank the anonymous referee for many useful comments.

REFERENCES

Bahcall J.N., Bergeron J., Boksenberg A. et al., 1996, ApJ., **457**, 19.

Bajtlik S., Duncan R.C., Ostriker J.P., 1988, ApJ., **327**, 570

Bardeen J.M., Bond J.R., Kaiser N., Szalay A., 1986, ApJ., **304**, 15

Bergeron J., Cristiani S., & Shaver P.A., 1992, A&A, **257**, 417

Bi H., & Davidsen A.F., 1997, ApJ., **479**, 523

Black J.H., 1981, MNRAS, **197**, 553

Bryan G.L., Machacek M., Anninos P., Norman M.L., 1999, **517**, 13

Bond J.R., Szalay A.S., & Silk J., 1988, ApJ., **324**, 627

Bond J.R., & Wadsley J.W., 1997, in "Structure and Evolution of the Intergalactic Medium from QSO Absorption Line Systems", eds. P.Petitjean, S. Charlot, p. 143.

Buryak O.E., Doroshkevich A.G., 1996, A&A., **306**, 1

Carswell R.F., Lanzetta K.M., Parnel H.C., & Webb J.K., 1991, ApJ., **371**, 36

Cen R., Ostriker J.P., 1993, ApJ., **404**, 415.

Connolly A.J., Szalay A.S., Romer A.K., et al., 1996, ApJ., **473**, L67

Cristiani S., D'Odorico S., Fontana A., et al., 1995, MNRAS, **273**, 1016.

Cristiani S., D'Odorico S., D'Odorico V., et al., 1996, MNRAS, **285**, 209

Cowie L., Songaila A., Kim T.S., & Hu E.M., 1995, AJ., **109**, 1522.

Davé R., Hernquist L., Katz N., Weinberg D.H., 1999, ApJ., **511**, 521,

Demiański M. & Doroshkevich A., 1999, MNRAS., **306**, 779, (DD99).

Demiański M., Doroshkevich A.G., & Turchaninov V.I., 1999, MNRAS, submitted, (Paper I)

Demiański M., Doroshkevich A.G., Müller V., & Turchaninov V.I., 1999, MNRAS, in press, (DDMT).

Dey A., & Chaffee F.H., 1998, ApJ. **498**, L93

Dinshaw N., Foltz C.B., Impey C.D., et al., 1995, Nature, **373**, 223.

Doroshkevich, A.G., Tucker, D.L., Oemler, A.A., et al., 1996, MNRAS, **283**, 1281. (LCRS1)

Doroshkevich A.G., Müller V., Retzlaff J., & Turchaninov V.I., 1999, MNRAS, **306**, 575, (DMRT).

Fan X., White R., Davis M., et al., 2000, astro-ph/0005414

Fardal M.A., & Shull J.M., 1993, ApJ., **415**, 524

Fernandes-Soto A., Lanzetta K.M., Barcon X., et al., 1996, ApJ. **460**, L85.

Giallongo E., Cristiani S., Fontana A., & Trevese D., 1993, ApJ., **416**, 137

Giavalisco M., Steidel C.C., Adelberger K.L., Dickinson M.E., Pettini M, Kellogg M., 1998, ApJ., **503**, 543

Governato F., Baugh C.M., Frenk C.S., et al. 1998, Nature, **392**, 389.

Hernquist L., Katz N., Weinberg D.H., Miralda-Escude J., 1996, ApJ., **457**, L51.

Hu E.M., Tae-Sun K., Cowie L., & Songaila A., 1995, AJ, **110**, 1526

Hui L., Gnedin N.Y., & Zhang Yu., 1997, ApJ, **486**, 599.

Ikeuchi S., Ostriker J.P, 1986, ApJ., **301**, 522.

Jenkins A., Frenk C.S., Pearce F.R. et al., 1998, ApJ., **499**, 20.

Kerscher M., 2000, in Proceedings of the Conference on Statistical Physics and Spatial Statistics (Wuppertal, Feb. 1999), eds. Mecke, K. and Stoyan, D., in press; astro-ph/9912329

Khare P., Srianand R., York D.G., et al., 1997, MNRAS, **285**, 167.

Kim T.S., Hu E.M., Cowie L.L.,& Songaila A., 1997, AJ., **114**, 1.

Kirkman D., & Tytler D., 1997, ApJ., **484**, 672.

Kulkarni V.P., Huang K., Green R., et al., 1996, MNRAS, **279**, 197

Lanzetta K.M., Bowen D.V., Tytler D., & Webb J.K., 1995, ApJ., **442**, 538.

Le Brune V., Bergeron J., & Boisse P., 1996, A&A, **306**, 691

Levshakov S.A., Kegel W.H., 1996, MNRAS, **278**, 497.

Levshakov S.A., Kegel W.H., 1997, MNRAS, **288**, 787.

Lu L., Sargent W.L.W., Womble D.S., Takada-Hidai M., 1996, ApJ., **472**, 509

Machacek M., Bryan G.L., Meiksin A., Anninos P. et al. 2000, ApJ., **532**, 118

McGill C., 1990, MNRAS, **242**, 544

Meiksin A., 1994, ApJ., **431**, 109

Melotte A.L., Shandarin S.F., Splinter R.J., Suto Y., 1997, ApJ., **479**, L79

Miralda-Escude J., Rees M.J., 1993, MNRAS., **260**, 616.

Miralda-Escude J., Cen R., Ostriker J.P., & Rauch M., 1996, ApJ., **471**, 582.

Morris S.L., Weymann R.J., Dressler A., et al., 1993, ApJ., **419**, 524

Nath B.B., 1997, ApJ., **482**, 621.

Nusser A., Haehnelt M., 1999, MNRAS, **303**, 179

Oort J.H., 1981, Astr.Astrophys., **94**, 359.

Oort J.H., 1984, Astr.Astrophys., **139**, 211.

Petitjean P., Mueket J.P., & Kates R.E., 1995, A&A , **295**, 9.

Quashnock J.M., Vanden Berk D.E., York D.G., 1996, ApJ., **472**, L69

Quashnock J.M., Vanden Berk D.E., York D.G., 1998, in

'Eighteenth Texas Symposium on Relativistic Astrophysics and Cosmology' "Texas in Chicago", eds. A.V.Olinto, J.A.Frieman & D.Schramm, World Scientific, p. 655.

Rauch M., Carswell R.F., Webb J.K., & Weymann R.J., 1993, MNRAS, **260**, 589.

Rauch M., Miralda-Escude J., Sargent W.L.W., et al., 1997, ApJ., **489**, 7.

Rees M.J., 1986, MNRAS, **218**, 25p.

Rees M.J., 1995, in Meylan J., ed., QSO Absorption Lines, p. 419.

Rodriguez-Pascual P.M., de la Fuente A., 1995, ApJ., **448**, 575.

Sargent, W.L.W., Young, P.J., Boksenberg, A. & Tytler, D., 1980, Ap.J.Suppl, **42**, 41

Sathyaprakash B.S., Sahni V., Shandarin S.F., 1998, ApJ, **508,** 551

Shandarin S., Zel'dovich Ya.B., 1989, Rev.Mod.Phys., **61**, 185

Shandarin S., Melotte A.L., McDavitt K., Pauls J.L., Tinker J., 1995, Phys.Rev.Let., **75**, 7

Shull J.M., Stocke J.T., Penton S.V., 1996, AJ, **111**, 72.

Splinter R.J., Melotte A.L., Shandarin S.F., Suto Y., 1998, ApJ, **497**, 38

Steidel C.C., Adlerberger K.L., Dickinson M., Giavalisco M., Pettini M., & Kellogg M., 1998, ApJ., **492**, 428.

Stocke J.T., Shull J.M., Penton S.V., et al., 1995, ApJ. **451** 24.

Tucker D.L., Oemler A.,Jr., Kirshner R.P., et al.,1997, MNRAS, **285**, L5

Theuns T., Leonard A., Efstathiou G., Pearce E.R., Thomas P.A., 1998, MNRAS, **301**, 478

Theuns T., Leonard A., Schaye J., Efstathiou G., 1999, MNRAS, **303**, 58

Tytler D., 1987, ApJ, **321**, 49

Tytler D., 1995, in Meylan J., ed., QSO Absorption Lines, p. 289.

Ulmer A., 1996, ApJ., **473**, 110

Valageas P., Schaeffer R., Silk J., 1999, AA, **345**, 691

van de Weygaert R., 1991, Ph.D. Thesis, University of Leiden

Webb J.K., 1987, in Hewett A., Burbidge G., Fang L.Z., eds., Proc. IAU Symp. 124, Observational Cosmology. Reidel, Dordrecht, p. 803

Weinberg D.H., Burles S., Croft R.A.C., et al., 1998, in "Evolution of Large Scale Structure: From Recombination to Garching", eds. A.J. Banday, R.K. Sheth, L.N. Da Costa, p. 346

Williger G.M., Baldwin J.A., Carswell R.F. et al., 1994, ApJ., **428**, 574

Williger G.M., Hazard C., Baldwin J.A., & McMahon R.G., 1996, ApJS., **104**, 145.

Zel'dovich, Ya.B., Novikov, I.D., 1983, The Structure and Evolution of the Universe, University of Chicago Press, Chicago.

Zel'dovich Ya.B., 1970, Astrophysica, **5**, 20

Zhang Yu., Anninos P., Norman M.L., Meiksin A., 1997, ApJ., **485**, 496

Zhang Yu., Meiksin A., Anninos P., Norman M.L., 1998, ApJ., **495**, 63

Zuo L, 1992, MNRAS, **258**, 36

Appendix A

COBE normalized power spectrum

A convenient universal normalization of the power spectrum can be obtained using the anisotropy of Microwave Background Radiation measured by COBE. The convenient parametrisation applied to open universe with matter density $\Omega_m \leq 1$ and for the spatially flat universe with $\Omega_m + \Omega_\Lambda = 1$ can be taken from Bunn & White (1996).

For the Harrison - Zel'dovich initial power spectrum with the BBKS transfer function we have:

$$\sigma_\rho^2(z) = 3\tau^2(z)\frac{m_0}{m_{-2}^2}, \qquad (A.1)$$

where a usual definition of moments of power spectrum is used:

$$m_n = \int_0^\infty x^{3+n} T^2(x) dx. \qquad (A.2)$$

The function $\tau(z) = \tau_0 B(z)$ depends on the model of the universe and can be expressed trough Ω_m & h as follows:

$$\Omega_m + \Omega_\Lambda = 1$$

$$B(z) \approx \left[\frac{1 - \Omega_m + 2.2\Omega_m(1+z)^3}{1 + 1.2\Omega_m}\right]^{-1/3},$$

$$(1+z)\tau(z) \approx 2.73h^2\Omega_m^{1.21}[0.45\Omega_m^{-1} + 0.55]^{1/3}, \; z \gg 1, \; (A.3)$$

and for $\Omega_m = 0.3, \; h = 0.6$ we have

$$(1+z)\tau(z) \approx 0.29.$$

For the open universe with $\Omega_\Lambda = 0, \quad \Omega_m \leq 1$

$$B^{-1}(z) \approx 1 + \frac{2.5\Omega_m}{1 + 1.5\Omega_m} z,$$

$$(1+z)\tau(z) \approx 1.1h^2\Omega_m^{0.65 - 0.19 ln\Omega_m}(1 + 1.5\Omega_m), \; z \gg 1 \; (A.4)$$

and, for example, for $\Omega_m = 0.5, \; h = 0.6$ we have

$$(1+z)\tau(z) \approx 0.4.$$

More details can be found in DD99 and DDMT.

Appendix B

Bulk heating and cooling of gas

The thermal evolution of gas is described by the well known equation

$$\frac{3}{2T}\frac{dT}{dt} = \frac{1}{n_b}\frac{dn_b}{dt} + \frac{\epsilon_\gamma \Gamma_\gamma n_{HI} - n_b^2(\beta_{fb} + \beta_{ff})}{n_b k_B T}, \qquad (B.1)$$

where ϵ_γ is the mean energy injected at a photoionization and radiative cooling coefficients for free-bound and free–free emissions can be taken as

$$\beta_{fb} \approx 3.7 \; 10^{-25}(T/10^4K)^{1/2} erg \; cm^3/s,$$

$$\beta_{ff} \approx 2 \cdot 10^{-25}(T/10^4K)^{1/2} erg \; cm^3/s.$$

If the ionization equilibrium is reached and

$$\alpha_{rec} n_b^2 = n_{HI}\Gamma_\gamma$$

then equation (B.1) can be rewritten more transparently as

$$\frac{3}{2Tn_b}\frac{dT}{dt} = \frac{1}{n_b^2}\frac{dn_b}{dt} + \beta_s(T_\gamma/T - 1), \qquad (B.2)$$

$$\beta_s = \frac{\beta_{fb} + \beta_{ff}}{k_B T} \approx 4.2 \cdot 10^{-13}(T/10^4K)^{-1/2} cm^3 s^{-1}$$

and $T_\gamma = (5 - 10) \cdot 10^4 K$ for the suitable spectrum of UV radiation (Black, 1981). T_γ depends on the spectrum of local radiation and can vary from point to point. This heating becomes negligible for the cold high density clouds when the radiative cooling due to the line emission is essential. For the main population of observed absorbers

$$b_{obs} \sim 25 - 30\text{km/s}, \quad T_{obs} \approx (4 - 6) \cdot 10^4 K \leq T_\gamma,$$

and the influence of bulk heating could be essential.

Eq. (B.2) can be suitably rewritten as follows:

$$\frac{d}{dt}\frac{T^{3/2}}{n_b} = T^{3/2}\beta_s(T_\gamma/T - 1), \qquad (B.3)$$

that allows us to integrate it directly. Using the definition of entropy function, F_S, as given by (2.20) we obtain:

$$F_S^{3/2}(z) = F_S^{3/2}(z_f) + \alpha_s \int_z^{z_f} dx \frac{H_0}{H(x)}\frac{T_\gamma(x) - T(x)}{(1+x)T_{bg}},$$

$$\alpha_s = 1.5h^{-1}\zeta^3\Theta_{bar}. \qquad (B.4)$$

where z_f is the redshift of pancake formation. This result is obtained under condition of ionization equilibrium. In the simplest case of fixed temperatures, $T(z) = \mathrm{const} \le T_\gamma(z) = \mathrm{const}$, we have

$$F_S^{3/2}(z) = F_S^{3/2}(z_f) + \alpha_s\ H_0[t(z) - t(z_f)]\frac{T_\gamma - T}{T_{bg}}, \quad (B.5)$$

that means the slow growth of entropy and drop of the density of absorbers and N_{HI}.

The influence of the bulk heating can be enhanced by the pancake disruption due to the clustering of both DM and baryonic components. This process is usually accompanied by the adiabatic reduction of temperature in expanded regions that accelerates the bulk heating. In this case, however, the parameters b and N_{HI} are strongly correlated. This means that the possible contribution of such heating is restricted at least for richer absorbers.